Two-Phase Approach for the Analysis of Laterally Loaded Pile Groups in Sandy Soils

Navid Nazeran[1] and Ehsan Seyedi Hosseininia, Aff.M.ASCE[2]

Abstract: In this study, a new hybrid method is suggested for the analysis of laterally loaded pile groups in sandy soils. In the proposed method, a pile group is replaced by an equivalent single pile (ESP) using the concept of two-phase material. Perfect bonding hypothesis and linear elastic behavior are assigned in the application of the two-phase approach. The ESP is analyzed by employing an appropriate single-pile *p-y* method to obtain a bending moment profile of the laterally loaded pile group. The proposed approach is evaluated by the results of full-scale and centrifuge experimental tests. Good agreements between measured and computed bending moment profiles approved the adequacy of the proposed approach. The properties of the ESP depend on the flexibility factor and slenderness of each pile, as well as pile spacing in the group. The effect of all these parameters is reflected in a factor named κ-multiplier. The effects of various parameters on the κ-multiplier is investigated by parametric studies. Generally, the proposed method provides a simple procedure to analyze the complicated problem of laterally loaded pile groups. **DOI: 10.1061/(ASCE)GM.1943-5622.0001821**. *© 2020 American Society of Civil Engineers*.

Author keywords: Pile group; Lateral loading; Two-phase approach; *p-y* method; Sand.

Introduction

Application of pile groups has grown in recent decades, owing to construction developments in different fields of industries, such as petroleum and offshore utilities. Pile groups are affected by lateral loads, such as winds, waves, ship impacts, and earthquakes and, hence, the analysis of laterally loaded piles is essential. Many experimental, analytical, and numerical studies have been conducted to understand the lateral behavior of pile groups, and several methods have been presented for analysis and design.

Analytical methods of laterally loaded pile groups can be generally classified into three categories: the continuum method, Winkler spring method, and hybrid method. In the continuum method, the soil around the piles is treated as a continuum with an associated stress–strain relationship. In the simplest form, it is assumed that the soil behavior is elastic and the pile group response is analyzed (e.g., El Sharnouby and Novak 1985; Poulos and Davis 1980; Randolph 1981). More-rigorous soil constitutive models can also be implemented by using finite element (e.g., Comodromos and Papadopoulou 2012; Teramoto et al. 2018; Wakai et al. 1999) and finite difference (e.g., Fayyazi et al. 2014) analyses. In the Winkler spring method, the pile is assumed to be an elastic beam that is attached to discrete springs, representing the soil. It is often assumed that the behavior of springs obeys a nonlinear relationship, i.e., *p-y* curves, between the soil resistance (p) and soil lateral displacement (y). Typical *p-y* curves for single piles, also known as the *p-y* method, are recommended by many researchers (e.g., Matlock 1970; Reese et al. 1974) and standards (API 2002; DNV 1977). The behavior of a pile group can be studied by introducing a *p*-multiplier (Brown et al. 1988) or reduction factor (Fayyazi et al. 2014) to modify *p-y* curves of single piles and, later, the piles in the group can be analyzed. The applicability of this method has been validated by experimental tests (e.g., Christensen 2006; McVay et al. 1995, 1998; Rollins et al. 2005; Ruesta and Townsend 1997; Tobita et al. 2004). The third approach is the hybrid method, which employs both the elastic continuum and *p-y* analysis methods (e.g., Leung and Chow 1987; Ooi and Duncan 1994), or uses the elastic theory for piles and treating the soil as springs (e.g., Kitiyodom and Matsumoto 2002, 2003). Other solutions such as variation approach (Shen and Teh 2002) and digital signal processing (Zhao and Wang 2018) have been applied for laterally loaded pile groups.

From a specific viewpoint, piles in a group can be considered as inclusions that reinforce the soil medium. According to Fig. 1, in a macroscopic view, the pile group and the among soil it can be regarded as a homogenous but anisotropic composite material, in which the piles are distributed periodically. For reinforced soil medium, de Buhan and Sudret (1999) introduced a so-called multiphase model as an extension of the classical homogenization technique. In the multiphase model, a composite material at the macroscopic scale is regarded not only as a single medium like the classical homogenization method, but also as a mutual superposition of interacting media called "phases," representing the soil and the inclusions. Appropriately, as shown in Fig. 1(b), a pile group can be considered as a two-phase material, in which each geometrical point consists of the superposition of the matrix phase (representative of soil) and reinforcement phase (representative of piles). Each phase has its own characteristics, with individual displacement and/or rotation fields. The two-phase approach has been applied to the analysis of rock-bolted tunnels (de Buhan et al. 2008; Sudret and de Buhan 2001) and reinforced soil walls (Seyedi Hosseininia and Ashjaee 2018; Seyedi Hosseininia and Farzaneh 2010a, b, 2011). Analysis of piled embankment (Hassen et al. 2009; Son et al. 2010), determination of horizontal and rocking impedances of pile groups (Nguyen et al. 2016), finite element simulations of the behavior of pile-raft foundations

[1]Ph.D. Candidate, Dept. of Civil Engineering, Ferdowsi Univ. of Mashhad, Mashhad 9177943369, Iran. ORCID: https://orcid.org/0000-0001-6140-6619. Email: navid_nazeran@mail.um.ac.ir

[2]Associate Professor, ASCE Affiliate member, Dept. of Civil Engineering, Ferdowsi Univ. of Mashhad, P.O. Box: 91775-11111, Mashhad 9177943369, Iran (corresponding author). ORCID: https://orcid.org/0000-0002-9810-8698. Email: eseyedi@um.ac.ir

Note. This manuscript was submitted on March 27, 2019; approved on June 4, 2020; published online on August 6, 2020. Discussion period open until January 6, 2021; separate discussions must be submitted for individual papers. This paper is part of the ***International Journal of Geomechanics***, © ASCE, ISSN 1532-3641.

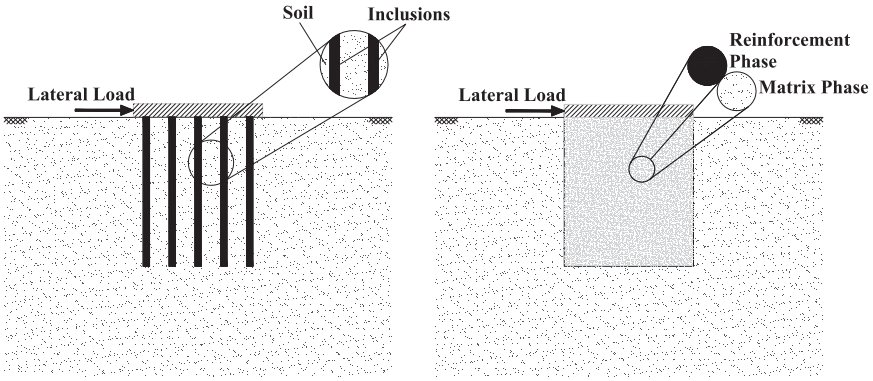

Fig. 1. Schematics of a laterally loaded pile group: (a) in a discrete form; and (b) as a two-phase material.

(Bourgeois et al. 2013), and settlement analysis accounting for soil–pile interactions (Bourgeois et al. 2012; Nasrollahi and Seyedi Hosseininia 2019) are other examples of using a two-phase approach to study piled structures.

In the present study, laterally loaded pile groups in sandy soils are analyzed by proposing a new hybrid method. In the proposed method, a pile group is replaced by an Equivalent Single Pile (ESP) by using the two-phase approach, which is analyzed with appropriate *p-y* curves. To validate the proposed hybrid method, computed results are compared with those of full-scale and centrifuge tests. This study focuses on the determination of bending moment profiles of pile groups under different lateral displacement levels. The effects of piles and soil properties on the results of the proposed method are investigated, as well.

Principles of Two-Phase Approach

Static equilibrium equations of a two-phase system were established in the framework of virtual works principle (de Buhan and Sudret 1999). The two-phase approach was developed to consider flexural and shear behavior of linear inclusions (de Buhan and Sudret 2000; Hassen and de Buhan 2005). A brief recall of the established equations in the framework of elastic constitutive law for each phase is introduced here. The equilibrium equations are

$$\mathrm{div}\boldsymbol{\sigma^m} + \rho^m \boldsymbol{F^m} - \boldsymbol{J} = \boldsymbol{0} \tag{1}$$

for the matrix phase, and

$$\begin{cases} div(n^r \boldsymbol{e_x} \otimes \boldsymbol{e_x} + v^r \boldsymbol{e_y} \otimes \boldsymbol{e_y}) + \rho^r \boldsymbol{F^r} + \boldsymbol{J} = \boldsymbol{0} \\ div(m^r \boldsymbol{e_z} \otimes \boldsymbol{e_x}) + v^r \boldsymbol{e_z} = \boldsymbol{0} \end{cases} \tag{2}$$

for the reinforcement phase. The superscripts *m* and *r* denote matrix and reinforcement phases, separately. Tensors and vectors in the above equations are specified with the boldface letters. In Eqs. (1) and (2), $\boldsymbol{\sigma^m}$ represents the classical Cauchy stress tensor defined in every point of the matrix phase. The term $\rho\boldsymbol{F}$ in both equations is the vector of the external body force applied to each phase. $\boldsymbol{J}$ denotes the interaction force vector exerted by the reinforcement phase over the matrix phase and vice versa. The terms n^r, v^r, and m^r are the densities of axial force, shear force, and bending moment per unit area, respectively. The terms $\boldsymbol{e_x}$, $\boldsymbol{e_y}$, and $\boldsymbol{e_z}$ are the unit vectors along the *x*-, *y*-, and *z*-axis, respectively. The sign $\otimes$ refers to the dyadic product of vectors. Fig. 2 illustrates all the stress tensor components, as well as force vectors with positive values. It is noted that the concept of anisotropic micropolar or Cosserat continuum has been also used in the modeling of the reinforcement

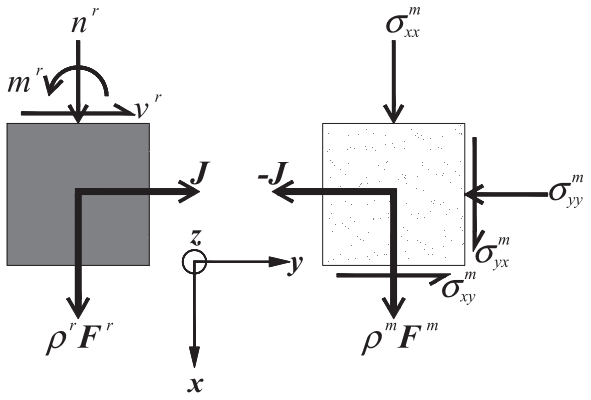

Fig. 2. Stress components and force vectors in a two-phase system. Signs are positive.

phase similar to the modeling of layered materials (Adhikary and Dyskin 1997) or beam lattices (Chen et al. 1998). Thus, the expression $n^r \boldsymbol{e_x} \otimes \boldsymbol{e_x} + v^r \boldsymbol{e_y} \otimes \boldsymbol{e_y}$ is a nonsymmetrical stress tensor by considering the shear force density and $m^r \boldsymbol{e_z} \otimes \boldsymbol{e_x}$ is the tensor of couple stress. For more details, see the reference Adhikary and Dyskin (1997). In order to obtain the solution of these equations, corresponding stress boundary conditions should be prescribed on the boundary surface of each phase individually.

Regarding the displacement fields of the two-phase system ($\boldsymbol{\xi^m}$, $\boldsymbol{\xi^r}$) in the context of linear elastic behavior and small deformations, the strain tensor ($\boldsymbol{\varepsilon^m}$) of the matrix phase is classically defined as

$$\boldsymbol{\varepsilon^m} = \frac{1}{2}\{\boldsymbol{grad\xi^m} + {}^t\boldsymbol{grad\xi^m}\} \tag{3}$$

and the constitutive elastic law under isotropic condition for the matrix phase (and also for the soil medium) is expressed as

$$\boldsymbol{\sigma^m} = \frac{2G^m \nu^m}{1-2\nu^m}(tr\boldsymbol{\varepsilon^m})\boldsymbol{I} + 2G^m\boldsymbol{\varepsilon^m} \tag{4}$$

where G^m and ν^m = shear modulus and Poisson's ratio of the matrix (and the soil), respectively. Eq. (4) is another form of the elastic constitutive law in terms of Lamé constants.

For the reinforcement phase, as regards the classical context of the individual Timoshenko beams, three strain variables, namely axial strain (ε^r), shear strain (θ^r), and curvature (χ^r), are introduced

by de Buhan and Sudret (2000):

$$\varepsilon^r = \frac{\partial \xi_x^r}{\partial x}, \quad \theta^r = \frac{\partial \xi_y^r}{\partial x} - \omega^r, \quad \chi^r = \frac{\partial \omega^r}{\partial x} \tag{5}$$

where ω^r = rotation field of the reinforcement phase. According to these strain variables, the scalar form of stress–strain relations in the framework of one-dimensional elastic behavior is obtained as

$$n^r = \alpha^r \varepsilon^r, \quad v^r = \beta^r \theta^r, \quad m^r = \gamma^r \chi^r \tag{6}$$

Similar to beam stiffness characteristics, α^r, β^r, and γ^r = axial, shear, and flexural stiffness densities per unit area of the pile group, respectively. For a pile as an inclusion with the properties of cross-section area A^I, moment of inertia I^I, elastic modulus E^I, and shear modulus G^I, these stiffness densities are defined as

$$\alpha^r = \frac{A^I E^I}{s^2}, \quad \gamma^r = \frac{E^I I^I}{s^2}, \quad \beta^r = \frac{A^{*I} G^I}{s^2} \tag{7}$$

where $A^{*I} = A^I/f_s$ = reduced cross section of the reinforcement and f_s = shape factor depending only on the cross-sectional shape of the reinforcement. For a thin-walled tube, circular, and rectangular cross sections, f_s is equal to 2, 10/9, and 6/5, respectively, which can be obtained from structural analysis (Popov 1998).

In this study, to avoid the complexity in the definition of the interaction stiffness tensor ($\boldsymbol{J}$), a perfect bonding between the phases is assumed. Hence, the kinematics of the matrix and reinforcement phases remain identical:

$$\boldsymbol{\xi} = \boldsymbol{\xi}^m = \boldsymbol{\xi}^r \tag{8}$$

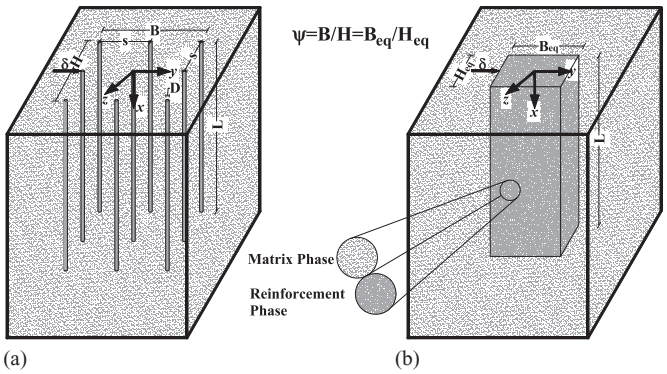

Fig. 3. Three-dimensional view of (a) a pile group; and (b) ESP as a two-phase system.

Application to Pile Group Problems

In the present approach, a single pile is analyzed by using a proper *p-y* curve that is equivalent to the whole of the pile group, whose properties are assessed by the two-phase model. The detailed problem-solving procedure is described in the next section.

Definition of the Problem

Fig. 3 schematically demonstrates a 3D view of a pile group in discrete and two-phase forms. In Fig. 3(a), arbitrary numbers of piles with the diameter D and length L are located along the x-axis in a regular arrangement with the specific distance s. In the yz plane, the pile group have the dimensions of B and H along the y- and z-axes, respectively. A horizontal displacement δ is applied to the pile group head along the y-axis. By considering the piles and the among soil as a two-phase system, the pile group can be converted to an ESP with a similar cross-sectional shape of the group with dimensions of B_{eq} and H_{eq} with the same similarity ratio $\psi = B/H = B_{eq}/H_{eq}$, as plotted in Fig. 3(b).

Fig. 4 demonstrates the 2D view of the pile group in the forms of a two-phase system and an ESP with specific boundary conditions. The discrete piles together with the among soil shown in Fig. 4(a) is replaced by a two-phase material in Fig. 4(b). The length of the reinforced-soil layer is L and the piles are located with the equal spacing s along the Ox direction. Boundary conditions for both phases are defined to be clamped at one end (the lower side) and pinned at the other end (the upper side). The ESP and the corresponding boundary conditions are depicted in Fig. 4(c). If the upper end of the pile group is imposed by a horizontal displacement δ, the displacement, as well as the rotation and curvature profiles of the corresponding two-phase system, can be obtained in the form of functions $f(x)$, $\omega(x)$, and $\chi(x)$, respectively.

The displacement field of the matrix phase $\boldsymbol{\xi}^m$ as well as the rotation ω^r and the curvature χ^r fields of the reinforcement phase can be defined based on the perfect bonding condition:

$$\boldsymbol{\xi}^m = \boldsymbol{\xi}^r = \boldsymbol{\xi} = f(x)\boldsymbol{e}_y, \quad \omega^r = \omega(x)\boldsymbol{e}_z, \quad \chi^r = \chi(x)\boldsymbol{e}_z \tag{9}$$

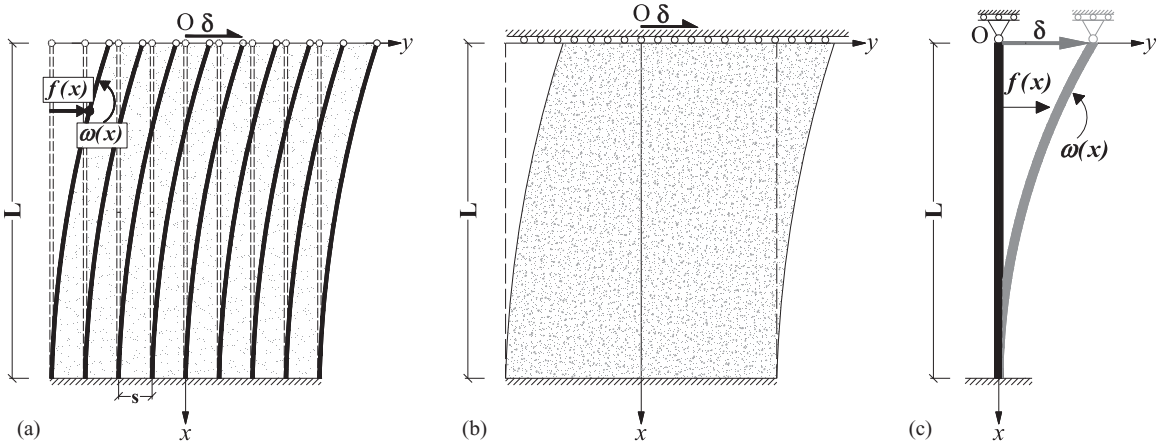

Fig. 4. Presentation of an elastic shear-loaded reinforced-soil layer with specific boundary conditions in the form of (a) discrete view; (b) two-phase system; and (c) a beam called as ESP, whose properties are equivalent to the pile group as a two-phase system.

It is assumed that the shear behavior of the piles (and the reinforcement phase accordingly) complies with that of a Timoshenko beam. For the two-phase system, the boundary conditions are

$$\begin{aligned} f(x=0)=\delta, \quad \chi(x=0)=0, \\ f(x=L)=0, \quad \omega(x=0)=0 \end{aligned} \tag{10}$$

The strain tensors of the matrix and the reinforcement phases are expressed in Eqs. (11) and (12), respectively:

$$\boldsymbol{\varepsilon^m}=\frac{f'(x)}{2}(\boldsymbol{e_x}\otimes\boldsymbol{e_y}+\boldsymbol{e_y}\otimes\boldsymbol{e_x}) \tag{11}$$

$$\varepsilon^r=0, \quad \theta^r=f'-\omega, \quad \chi^r=\omega' \tag{12}$$

According to Eqs. (4) and (6), the corresponding stress tensors are

$$\boldsymbol{\sigma^m}=2G^m\boldsymbol{\varepsilon^m}=G^m f'(x)(\boldsymbol{e_x}\otimes\boldsymbol{e_y}+\boldsymbol{e_y}\otimes\boldsymbol{e_x}) \tag{13}$$

$$\begin{aligned} n^r(x)=0, \quad v^r=\beta^r(f'-\omega), \\ m^r(x)=\gamma^r\chi(x)=\gamma^r\omega'(x) \end{aligned} \tag{14}$$

Substituting Eqs. (13) and (14) into the equilibrium equations [Eqs. (1) and (2)] in the absence of the external body forces yields

$$\begin{cases} G^m f'''(x)\boldsymbol{e_y}-\boldsymbol{J}=\boldsymbol{0} \\ \beta^r(f''(x)-\omega'(x))\boldsymbol{e_y}+\boldsymbol{J}=\boldsymbol{0} \\ (\gamma^r\omega''(x)+\beta^r(f'(x)-\omega(x))\boldsymbol{e_z}=\boldsymbol{0} \end{cases} \tag{15}$$

The elimination of $\boldsymbol{J}$ leads to the following differential equation:

$$\begin{cases} \omega'''(x)-\dfrac{\eta_1^2}{L^2}\omega'(x)=0 \\ f'(x)=\omega(x)-\dfrac{\eta_2^2}{\eta_1^2}L^2\omega''(x) \end{cases} \tag{16}$$

in which, nondimensional parameters, η_1 and η_2, are

$$\eta_1=\sqrt{\frac{G^m\beta^r L^2}{(G^m+\beta^r)\gamma^r}}; \quad \eta_2=\sqrt{\frac{G^m}{G^m+\beta^r}} \tag{17}$$

The solution of the differential Eq. (16) in general form is

$$\begin{cases} f(x)=A_1+A_2x+(1-\eta_2^2)\dfrac{L}{\eta_1}\left[A_3\sinh\left(\eta_1\dfrac{x}{L}\right)+A_4\cosh\left(\eta_1\dfrac{x}{L}\right)\right] \\ \omega(x)=A_2+A_3\cosh\left(\eta_1\dfrac{x}{L}\right)+A_4\sinh\left(\eta_1\dfrac{x}{L}\right) \end{cases} \tag{18}$$

where A_1, A_2, A_3, and A_4 are constants. By considering boundary conditions [Eq. (10)], horizontal displacement, rotation and curvature functions of the two-phase system is assessed as

$$\begin{cases} f(x)=\delta\dfrac{(1-\eta_2^2)[\sinh(\eta_1 x/L)-\sinh\eta_1]+\eta_1(1-x/L)\cosh\eta_1}{\eta_1\cosh\eta_1-(1-\eta_2^2)\sinh\eta_1} \\ \omega(x)=\delta\dfrac{\eta_1}{L}\dfrac{\cosh\eta_1-\cosh(\eta_1 x/L)}{\eta_1\cosh\eta_1-(1-\eta_2^2)\sinh\eta_1} \\ \chi(x)=-\delta\dfrac{\eta_1^2}{L^2}\dfrac{\sinh(\eta_1 x/L)}{\eta_1\cosh\eta_1-(1-\eta_2^2)\sinh\eta_1} \end{cases} \tag{19}$$

The absolute value of the bending moment per unit area (m^r) in the reinforcement phase is calculated by virtue of the curvature function (χ):

$$m^r(x)=\gamma^r\chi(x)=\gamma^r\delta\frac{\eta_1^2}{L^2}\frac{\sinh(\eta_1 x/L)}{\eta_1\cosh\eta_1-(1-\eta_2^2)\sinh\eta_1} \tag{20}$$

Substituting the definition of γ^r in Eq. (20) leads to the bending moment function $M^r(x)$ in the reinforcement phase as

$$\begin{aligned} M^r(x)&=m^r(x)\cdot s^2=E^I I^I\chi(x) \\ &=E^I I^I\delta\frac{\eta_1^2}{L^2}\frac{\sinh(\eta_1 x/L)}{\eta_1\cosh\eta_1-(1-\eta_2^2)\sinh\eta_1} \end{aligned} \tag{21}$$

In common practice, it is assumed that piles in the pile group behave like an Euler–Bernoulli beam, which means that shear deflections are negligible if subjected to lateral loads. This condition implies that the shear deflection is ignored ($\theta^r=0$) or the shear stiffness of the reinforcement phase (β^r) tends to infinity. Accordingly, the parameter η_2 reaches zero and the parameter η_1 tends to a dimensionless value called as relative stiffness density per unit area (η) of the pile group:

$$\eta=\sqrt{\frac{G^m}{\gamma^r}}L \tag{22}$$

In the case of the Euler–Bernoulli beam theory for the reinforcement phase, the bending moment profile has the following form:

$$\begin{aligned} M^r(x)&=m^r(x)\cdot s^2=E^I I^I\chi(x) \\ &=E^I I^I\delta\frac{\eta^2}{L^2}\frac{\sinh(\eta x/L)}{\eta\cosh\eta-\sinh\eta} \end{aligned} \tag{23}$$

Equivalent Single Pile (ESP)

The shear-loaded two-phase system described is considered as an ESP, which is a single beam under lateral displacement (δ) with fixed and pinned boundary conditions at the ends as illustrated in Fig. 4(c). This beam is characterized by the length L, elastic modulus (E_{eq}), and moment of inertia about the z-axis (I_{eq}) in terms of the dimensions B_{eq} and H_{eq}. Similarly, by considering a beam as a one-phase system ($G^m=0$) in Eq. (17) and resolving Eq. (16), the horizontal displacement f^{ESP}, the rotation ω^{ESP}, and the curvature χ^{ESP} functions of the ESP as a Timoshenko beam are obtained as

$$\begin{cases} f^{\text{ESP}}(x)=\dfrac{\delta}{2+6R/L^2}\left[\left(\dfrac{x}{L}\right)^3-\left(3+\dfrac{2R}{L^2}\right)\left(\dfrac{x}{L}\right)+2+\dfrac{6R}{L^2}\right] \\ \omega^{\text{ESP}}(x)=\dfrac{3\delta}{L(2+6R/L^2)}\left[\left(\dfrac{x}{L}\right)^2-1\right] \\ \chi^{\text{ESP}}(x)=\dfrac{6\delta}{L^2(2+6R/L^2)}\left(\dfrac{x}{L}\right) \end{cases} \tag{24}$$

where $R=(E_{\text{eq}}I_{\text{eq}}/G_{\text{eq}}A^*_{\text{eq}})$ represents the shear behavior contribution in the ESP in which A^*_{eq} and G_{eq} are the reduced cross section and shear modulus of the ESP, respectively. Assuming a rectangular cross section; i.e., $f_s=6/5$ for the ESP, the curvature function (χ^{ESP}) in Eq. (24) is simplified to

$$\chi^{\text{ESP}}(x)=\frac{\delta}{L^2}\frac{36(L/B_{\text{eq}})^2}{12(L/B_{\text{eq}})^2+5(1+\nu_{\text{eq}})}\left(\frac{x}{L}\right) \tag{25}$$

Int. J. Geomech., 2020, 20(10): 04020182

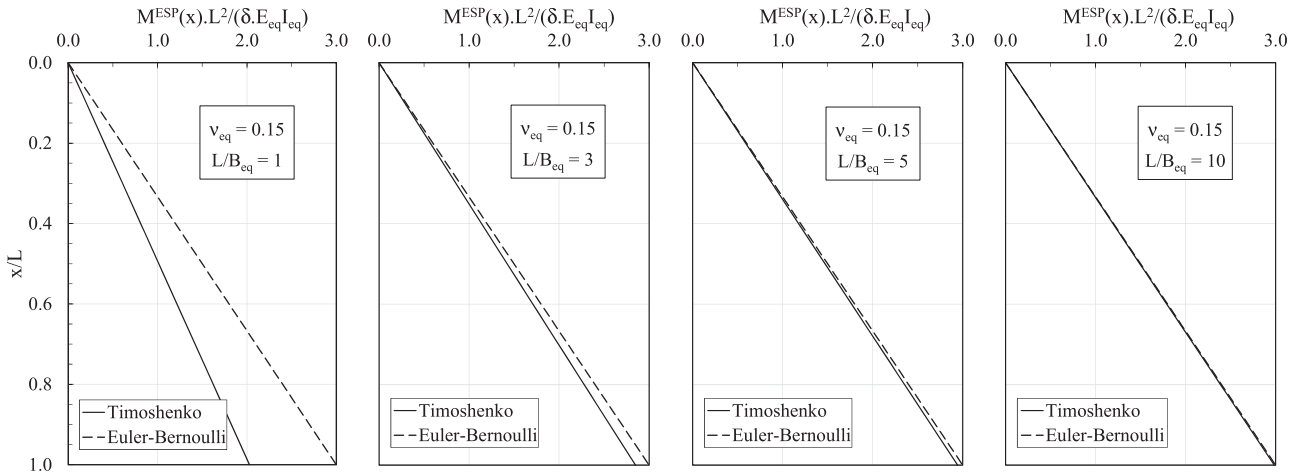

Fig. 5. Variations of dimensionless bending moment function of a laterally loaded ESP with normalized length considering Euler–Bernoulli and Timoshenko beam theories.

where ν_{eq} = Poisson's ratio of the ESP. Accordingly, the bending moment function (M^{ESP}) is determined as

$$M^{ESP}(x) = E_{eq}I_{eq} \cdot \chi^{ESP}(x) = E_{eq}I_{eq}\frac{\delta}{L^2}\frac{36(L/B_{eq})^2}{12(L/B_{eq})^2 + 5(1+\upsilon_{eq})}\left(\frac{x}{L}\right) \quad (26)$$

In the analysis of the laterally loaded ESP by using the *p-y* method, the shear behavior distribution is ignored so that the ESP converts to an Euler–Bernoulli beam. Assuming that the shear rigidity ($G_{eq}A^*_{eq}$) tends to infinity [and R tends to zero in Eq. (24)], the bending moment profile of an Euler–Bernoulli ESP is assessed by

$$M^{ESP}(x) = E_{eq}I_{eq} \cdot \chi^{ESP}(x) = E_{eq}I_{eq}\frac{3\delta}{L^2}\left(\frac{x}{L}\right) \quad (27)$$

To investigate the effect of the ESP geometry (and slenderness) on the behavior, the bending moment functions of both Euler—Bernoulli and Timoshenko ESPs are compared. The variation of the dimensionless bending moment functions of the ESPs, $M^{ESP}(x) \cdot L^2/(\delta \cdot E_{eq}I_{eq})$ along the normalized length (x/L) is depicted in Fig. 5 for values of $L/B_{eq} = 1$, 3, 5, and 10. For the Timoshenko ESP, $\nu_{eq} = 0.15$ is assumed. It is generally seen that the bending moments of the two ESPs get closer as the L/B_{eq} becomes bigger, such that for $L/B_{eq} = 3$, the maximum difference is about 6% at the fixed-end support ($x/L = 1$). It can be said that if the geometry of the ESP is configured such that $L/B_{eq} > 3$, then the ESP can be regarded as slender enough to ignore the effect of shear deflections on the behavior.

The properties of the ESP can be derived based on the characteristics of the two-phase system described before. The bending rigidity of the ESP, $(EI)_{eq}$, is calculated by equating the bending moment of the ESP and that of the two-phase system at the fixed end support ($x = L$):

$$(EI)_{eq} = E^I I^I \cdot \kappa \quad (28)$$

in which, a parameter named as κ-multiplier is defined as

$$\kappa = \frac{\eta^2}{3}\frac{\tanh\eta}{\eta - \tanh\eta} \quad (29)$$

The κ-multiplier can be interpreted as a magnification factor (greater than unity), which translates the bending rigidity of a single pile as a microscopic element to that of an ESP in a macroscopic view representing the pile group. The κ-multiplier is a function of the η parameter containing the properties of the pile group and the soil amongst according to Eq. (22). By applying a *p-y* model for the analysis of the ESP, the complicated problem of a laterally loaded pile group converts to a simple problem.

The application of the *p-y* method for the ESP as a single pile is achieved by solving the equations for a beam resting over a foundation (Hetenyi 1946). If the ESP is subdivided into incremental elements, the differential equation of the problem can be converted into a deference form and it can be solved numerically, as described in details by Reese and Van Impe (2010). Isenhower et al. (2018) have developed a computer software named LPILE that is widely used for single-piles analysis. By solving the equations, the bending moment along the length of the ESP can be obtained accordingly. Based on the concept of the ESP as a representative of the pile group, the bending moment profile of the ESP is equal to the sum of the bending moment profiles of all the rows of the pile group.

A challenging issue in the proposed simplified approach is the boundary condition at the tip of the ESP. This boundary condition refers to the situations where the tips of the piles penetrate into a dense soil layer or bedrock. It is worth mentioning that in the analysis of laterally loaded piles, there is always a point of fixity somewhere above the pile tip. The depth of the fixity in sandy soils depends on the bending rigidity of the piles and lateral subgrade modulus (Chen 1997) or piles diameter and lateral subgrade modulus (Caltrans 1990). Although there are some suggested relations in the literature to calculate the depth of fixity, the total length of the piles is considered here to avoid the confusion of selecting the best choice for the depth of fixity. Validation case studies explained in the following sections indicate that this assumption would be acceptable without loss of generality.

Step-by-Step Procedure for the Problem-Solving

A step-by-step process is presented here in order to investigate the response of a laterally loaded pile group in sandy soils by using the proposed approach. Fig. 6 demonstrates an arbitrary $n \times m$ pile group and the corresponding ESP in a *x-y-z* coordinate system located in a multilayered soil profile. The pile group is loaded by a lateral displacement, δ, at the head. The soil profile consists of N layers with different properties of thickness (h_1 to h_N), shear modulus (G^m_1 to G^m_N), unit weight (γ_1 to γ_N), internal friction angle (ϕ_1 to ϕ_N), and lateral subgrade modulus (k_1 to k_N). Pile spacing in the

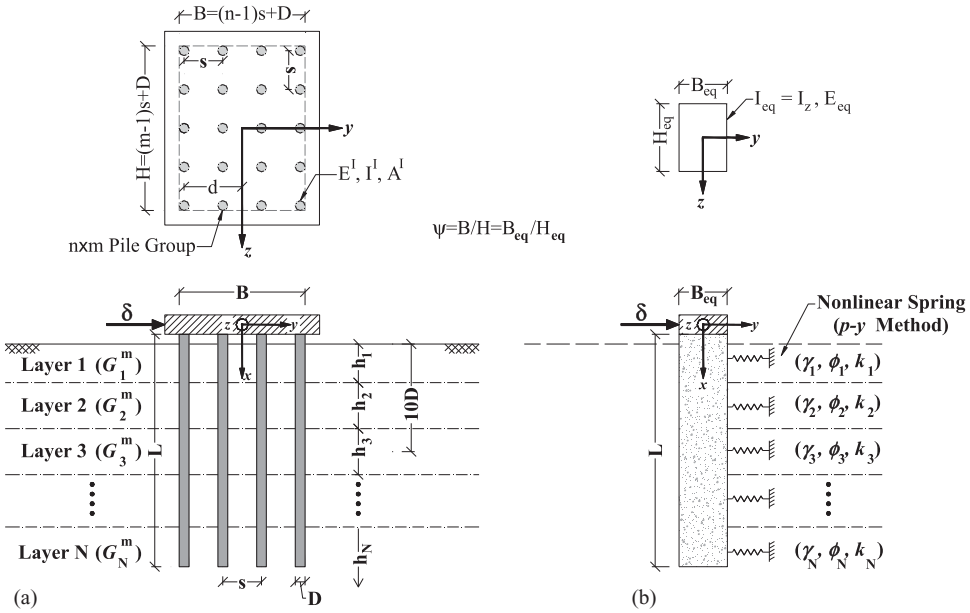

Fig. 6. A graphical scheme of the proposed hybrid approach for the analysis of a laterally loaded pile group located in a multilayered soil profile: (a) the pile group; and (b) the ESP.

group is equal to s in both the y- and z-directions. The piles are characterized by length (L), moment of inertia (I^I), cross-section area (A^I), and the elastic modulus (E^I). Back-to-back dimensions of the pile group in the front and leading rows are B and H in the y- and z-direction, respectively. The neutral axis of the pile group is located along the z-direction and the distance between the neutral axis and each pile row axis is d. The pile group and the soil amongst [Fig. 6(a)] can be replaced by an ESP and nonlinear springs, as illustrated in Fig. 6(b). The length of the ESP is equal to L and its dimensions in the plan view are B_{eq} and H_{eq} in the y- and z-direction, respectively. Other properties of the ESP are the moment of inertia about the z-axis (I_{eq}) and the elastic modulus (E_{eq}). The details and the steps of the analysis procedure are listed as:

1. The properties of the matrix phase (the soil equivalently) including shear modulus (G^m) and internal friction angle (ϕ) is estimated by using field tests data and/or empirical correlations. Lateral subgrade modulus (k) is also required for p-y analysis, which can be determined by the recommended diagram of API (2002). The correctness of the selected soil parameters can be assured by the analysis of a single pile if there is a good match between the bending moment profile obtained from analysis and measurement.
2. By knowing that the soil among the piles does not have any bending resistance, the moment of inertia of the ESP (I_{eq}) is calculated based on the arrangement of the piles in the group by having the neutral axis [z-axis in Fig. 6(a)] as well as the moment of inertia of each pile (I^I).
3. The elastic modulus of the ESP (E_{eq}) is computed as

$$E_{eq} = \frac{\kappa \cdot E^I I^I}{I_{eq}} \tag{30}$$

For the case where the pile group is located in layered soils (as shown in Fig. 6), different values of E_{eq} are obtained for each layer. In this case, it is suggested to use the weighted average value ($\bar{E}_{eq}$) with respect to the soil layer thickness up to the depth of 10 pile diameters. According to Brown et al. (1988), the pile response under lateral loading is dominated by a sandy soil layer with an effective depth of 10D.

4. The cross-section geometry of the ESP is regarded similar to that of the real pile group according to the piles arrangement and, hence, the dimensions of the ESP cross section is assessed. For instance, for a pile group where the piles are located in a rectangular pattern according to Fig. 6, the length (H_{eq}) and width (B_{eq}) of the ESP is obtained by

$$H_{eq} = \sqrt[4]{\frac{12 I_{eq}}{\psi}}, \quad B_{eq} = \psi H_{eq} \tag{31}$$

where $\psi = (B/H)$. It means that the global cross-section shape of the ESP is assumed to be similar to that of the real group pile, with the similarity ratio ψ.

5. As the last step, the ESP is analyzed by using the p-y curves that have been already validated for a single pile of the pile group. As a result, the bending moment profile of the pile group can be obtained. It is noted that the computed bending moment of the ESP is equal to the sum of the bending moment of all rows of the pile group which is conventionally reported in the literature.

In the application of p-y curves, there are various ideas in the literature about the relationship between the lateral subgrade modulus (k) and pile diameter (D). For instance, Terzaghi (1955), Vesic (1961), Reese et al. (1974), and Ashford and Juirnarongrit (2003), among others, believe that the lateral subgrade modulus is independent of the pile diameter, though there is an opposite opinion (e.g., Pender 1993; Poulos 2018) that states that the subgrade modulus has a reciprocal relationship with the pile diameter. Also, Meyer and Reese (1979) declared that for sandy soils, the value of the subgrade modulus is not a sensitive parameter in the analysis of lateral pile response, especially in terms of maximum bending moment. To avoid complexity in the problem-solving procedure and to extend the applicability of the proposed method, in the present study it is assumed that the lateral subgrade modulus is independent of pile diameter.

Int. J. Geomech., 2020, 20(10): 04020182

Table 1. Soil profile properties in the Rollins et al. (2005) study

Depth (m)	Soil type	γ' (kN/m^3)	E^m (MPa)	ν^m	c (kPa)	ϕ (°)	k (MN/m^3)	ε_{50} (strain)
0.00–0.51	Sand	10.3 (19.5)*	10 (27)	0.3	0	33	15.4 (24.4)	—
0.51–2.59	Sand	10.3	10	0.3	0	33	15.4	—
2.59–4.73	Sand	10.3	10	0.3	0	32	13.6	—
4.73–7.49	Sand	10.3	8	0.3	0	30	10.6	—
7.49–9.25	Soft clay	9.5	11.5	0.45	19.2	0	—	0.01
9.25–10.16	Sand	10.3	2	0.3	0	30	10.6	—
10.16–11.84	Soft clay	9.5	11.5	0.45	19.2	0	—	0.01

Note: Values in the parentheses indicates the soil properties in the moist condition (single pile testing).

Similar to other methods applied in the analysis of laterally loaded pile groups, the proposed hybrid method have its own advantages and limitations. The advantages can be listed as:

- The analysis procedure is easier with respect to other existing simplified methods. In the proposed hybrid method, only a single pile (ESP) is analyzed by using the p-y method, while in other pile group analyses it is required to analyze individually each pile row with a specific p-y curve by defining a p-multiplier (e.g., Rollins et al. 2005; Walsh 2005; Zhang et al. 1999).
- The hybrid method presented in this paper is more convenient than the numerical continuum methods, such as finite element and finite difference methods, because does not require modeling the whole pile group in detail.

The limitations of the proposed hybrid approach are:

- The bending moment of each row of the pile group cannot be calculated directly. As explained before, the present approach only gives the sum of the bending moment of the whole pile group, and an estimation of the value of each row can be attained instead. Meanwhile, by reviewing experimental and physical full-scale tests in the literature (e.g., Rollins et al. 2005; Tobita et al. 2004; Walsh 2005), the value of bending moments of each row of the pile groups have been reported to be almost the same or with small deviations from each other.
- The present approach is only applicable for the cases where the geometry of the pile group satisfies the condition of a slender ESP, i.e., $L/B_{eq} > 3$ since the p-y analysis is appropriate for long and thin piles.
- It is assumed that the behavior of the piles in the group and the soil amongst (and consequently the ESP) remains elastic during the analysis. Thus, this approach is not appropriate for large deformations or where the piles have plastic behavior.

Model Validations

In order to evaluate the proposed method, three experimental studies including two full-scale tests and one centrifuge test are considered here. The full-scale tests were carried out in the layered sandy soils with clayey lenses, and the centrifuge test was performed in a uniform sandy soil. In this section, a bending moment profile for each pile group is assessed by applying the proposed method. It is noted that the bending moment profile of the pile groups reported in the case studies was presented for each row. Hence, in order to have comparable results, the sum of the bending moment profile of all the rows is introduced as the bending moment profile of the pile group. The details of the tests and verification procedure are described next.

Case Study 1 (Physical Full-Scale Test)

Rollins et al. (2005) performed lateral load tests on a 3×3 pile group as well as on a single pile. The pipe piles had an approximate length $L = 12$ m, the outer diameter $D = 0.324$ m, and the wall thickness $t = 0.0095$ m. The moment of inertia of each pipe pile was $I^I = 1.43 \times 10^{-4}$ m^4 by considering the effect of attached equipment. The piles were located in 3.3D ($s = 1.07$ m) spacing in the group. The piles were made up of steel with an elastic modulus $E^I = 200$ GPa. Lateral loads were applied at a height of 0.69 and 0.86 m above the ground surface in the single pile and pile group tests, respectively.

The piles were driven into a layered soil profile including loose to medium-dense submerged sand underlain by clay. Rollins et al. (2005) estimated soil properties based on in situ standard penetration test (SPT) excluding soil elastic modulus and Poisson's ratio. To approximate the latter parameters, the graph presented by Callanan and Kulhawy (1985) is used. In the absence of SPT data for clayey layers, the elastic modulus is estimated by $E^m = 4q_c$ (Bowles 1996) in which, q_c is the cone resistance in the cone penetration test (CPT). Poisson's ratio for sandy and clayey layers are assumed as $\nu^m = 0.3$ and 0.45, respectively. Table 1 summarizes soil properties for each layer. The groundwater table in the single pile testing was about 0.5 m below the ground surface, but in pile group tests it rose to within about 0.1 m because of rainfall. The values written in the parentheses for some soil properties in Table 1 are related to the single pile tests (moist) condition.

Fig. 7 shows the measured as well as computed bending moment profiles of the single pile under different pile-head horizontal displacements, $\delta = 4.7$, 12.0, 20.7, and 30.5 mm. The circles in the figure indicate the measured moment values along the pile length and the solid lines show the predicted moment of the pile by using the p-y analysis. The analyses have been performed by implementing Reese et al. (1974) and Matlock's (1970) p-y curves for sand and clay, respectively. As shown, there is generally acceptable agreement between the experimental and analytical results, which means that the soil properties have been chosen properly.

The behavior of the pile group under lateral load is investigated by using the proposed ESP concept. Knowing that the cross section of the pile group is square ($B = H = 2.462$ m), the moment of inertia of the ESP (I_{eq}) is calculated as $I_{eq} = 0.06567$ m^4, leading to equivalent dimensions $B_{eq} = H_{eq} = 0.942$ m. The slenderness of the ESP is characterized by $L/B_{eq} = 12.8 \gg 3$, which satisfies the applicability of the proposed approach. The elastic modulus of the ESP (E_{eq}) is then calculated based on Eq. (30). Since the pile group is installed in the layered soil, different values of E_{eq} is obtained for each layer until the depth of 10D and the weighted average value is $\bar{E}_{eq} = 877$ MPa.

Fig. 8 illustrates the results of the analysis of the ESP with similar p-y models in terms of bending moment profiles. The pile group was laterally loaded under different levels of displacements, $\delta = 10$, 21, 29, and 39 mm. As shown, there is high correspondence between the measured and computed values of the bending moments along the depth. In all the tests, the value, as well as the depth of maximum bending moment, are suitably estimated. It seems that for larger lateral displacements, the bending moment is

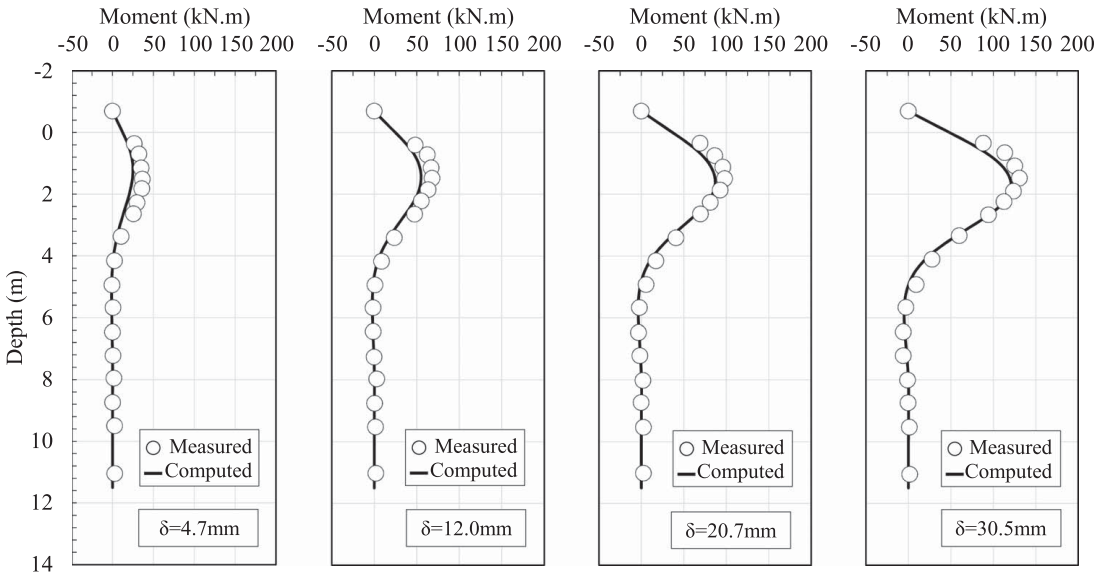

Fig. 7. Comparison of measured and computed bending moments versus depth at different pile-head deflections for the single pile test performed by Rollins et al. (2005).

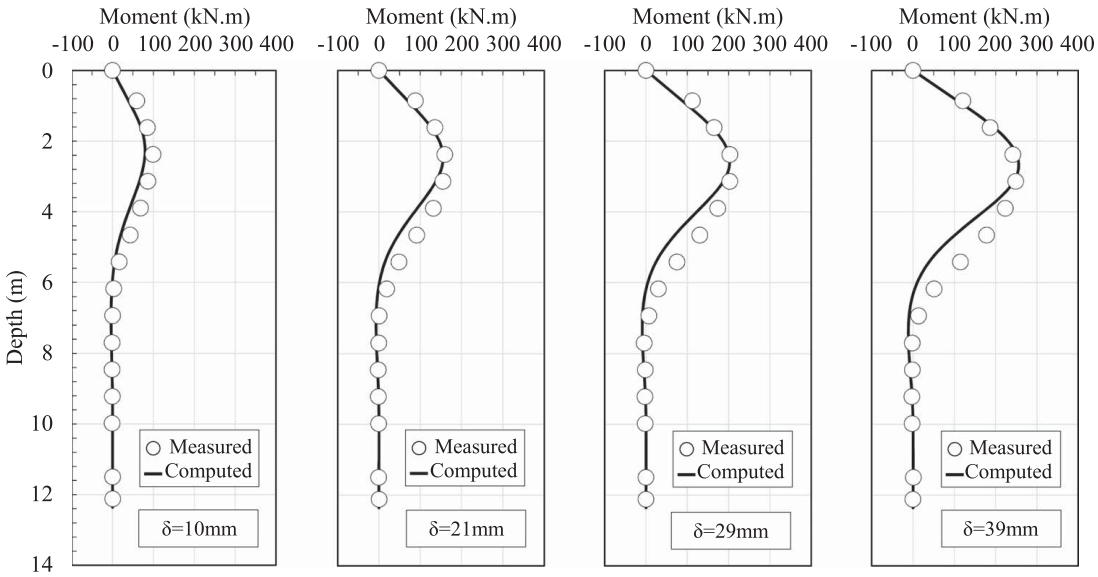

Fig. 8. Comparison of bending moments profiles measured in a full-scale test on a 3 × 3 pile group (Rollins et al. 2005) and computed bending moments profiles using the proposed method for different pile-head deflections.

underpredicted at the depths below the maximum value. However, there is again a good match for longer depths of the pile group.

Case Study 2 (Physical Full-Scale Test)

A 3 × 5 pile group and a single pile with identical characteristics were tested by Walsh (2005). The 13.5 m-length steel pipe piles were used with the same properties of those mentioned in the tests of the first case study reported by Rollins et al. (2005). Pile spacing in the group was equal to 3.92D ($s = 1.27$ m). The lateral load was applied at the height of 0.48 m above the ground surface in all the tests.

The piles were driven into a layered ground consisting of sandy soils in the top layers and soft clays at deeper layers, with an average relative density $D_r = 50\%$. The properties of the soil layers including γ', ϕ, c, k, and ε_{50} were estimated based on back analysis. It seems that the soil parameters ϕ and k are overestimated with respect to $D_r = 50\%$ (e.g., $\phi = 40°$ (Walsh 2005)) and thus, the values are revised in this study. The values of ϕ and k for sandy layers are approximated by the ϕ-k-D_r graph recommended by API (2002). The average values of E^m for each layer of the soil profile are derived from CPT results. Poisson's ratios are assumed to be $v^m = 0.3$ and 0.45 for sand and clay, respectively. Table 2 summatizes soil properties for each layer.

In order to check the correctness of the selected soil parameters, the behavior of the single pile is analyzed by using Reese et al. (1974) and Matlock's (1970) p-y models for sandy and clayey layers, respectively. Bending moment responses for different pile-head displacements $\delta = 6$, 13, 19, 25, and 38 mm are assessed and compared with the recorded results, as shown in Fig. 9. Generally, there is a good trend in the variation of the pile bending moment along the depth. An inconsistency is observed regarding the estimation of the magnitude or depth of maximum bending

Table 2. Soil profile properties in Walsh's (2005) study

Depth (m)	Soil type	γ' (kN/m^3)	E^m (MPa)	ν^m	c (kPa)	ϕ (degrees)	k (MN/m^3)	ε_{50} (strain)
0.0–2.1	Sand	16.7	48	0.3	0	33	24.4	—
2.1–2.4	Sand	6.8	28	0.3	0	33	15.4	—
2.4–2.7	Soft clay	9.1	12	0.45	41	0	—	0.01
2.7–3.7	Soft clay	9.1	12	0.45	50	0	—	0.01
3.7–4.6	Soft clay	9.1	8	0.45	40	0	—	0.01
4.6–6.3	Sand	8.1	40	0.3	0	32	13.6	—
6.3–8.0	Soft clay	9.1	12	0.45	57	0	—	0.01
8.0–14.0	Sand	6.7	20	0.3	0	30	10.6	0

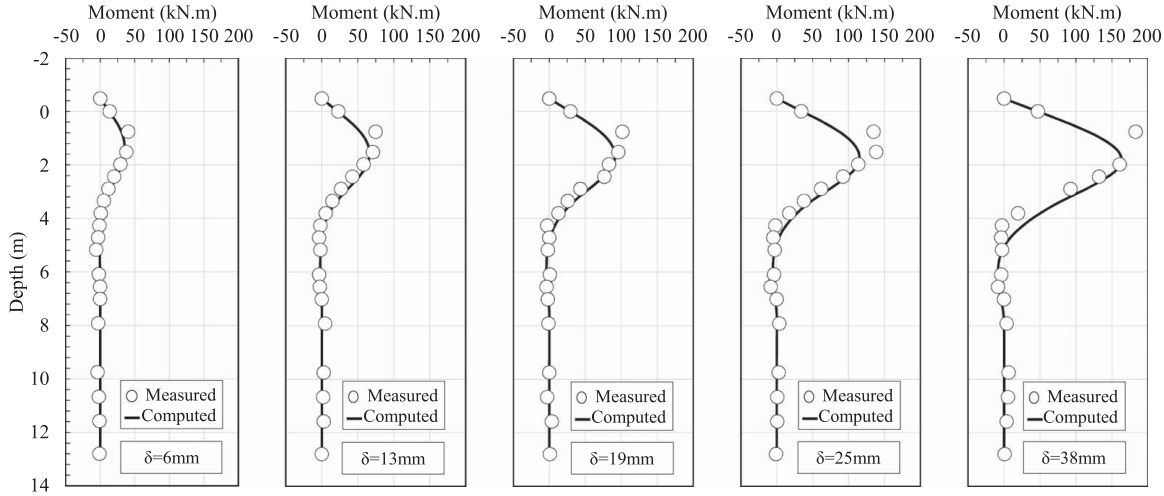

Fig. 9. Comparison of measured and computed bending moments versus depth at different pile-head deflections for the single pile test performed by Walsh (2005).

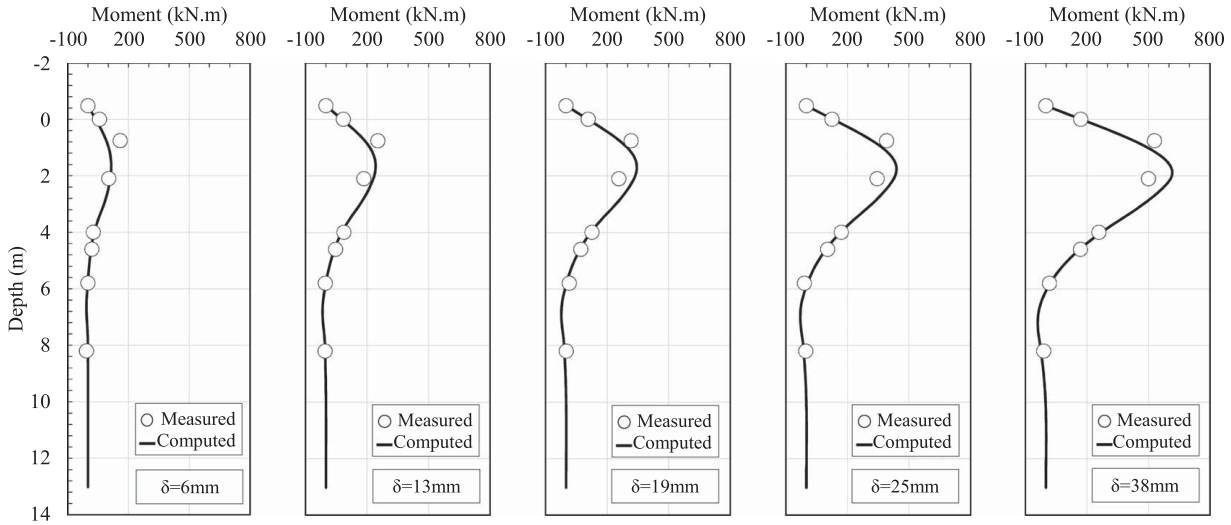

Fig. 10. Comparison of bending moments profiles measured in a full-scale test on a 3 × 5 pile group (Walsh 2005) and computed bending moments profiles by using the proposed method for different pile-head displacements.

moment. As explained by Walsh (2005), existence of malfunctioned gauges in some depth and interpolating the data with the gauges above and below a specific depth might be the reason of the differences between the measured and computed values of bending moment around the maximum bending moment.

In order to analyze the 3 × 5 pile group, the moment of inertia of the ESP is calculated as $I_{eq} = 0.15356$ m^4. Based on the pile arrangement in a rectangular area of the pile group with $\psi = B/H = 1.887$, the equivalent dimensions are $B_{eq} = 0.994$ m and $H_{eq} = 1.876$ m. Having calculated the I_{eq}, the equivalent elastic modulus (E_{eq}) of each soil layer is assessed and the weighted average value is obtained as $\bar{E}_{eq} = 897$ MPa. The L/B_{eq} ratio for the ESP is 13.6, which indicates that the proposed approach is appropriate for the analysis of this problem.

Fig. 10 shows the variation of measured and computed values of the bending moment of the pile group along the depth for the same

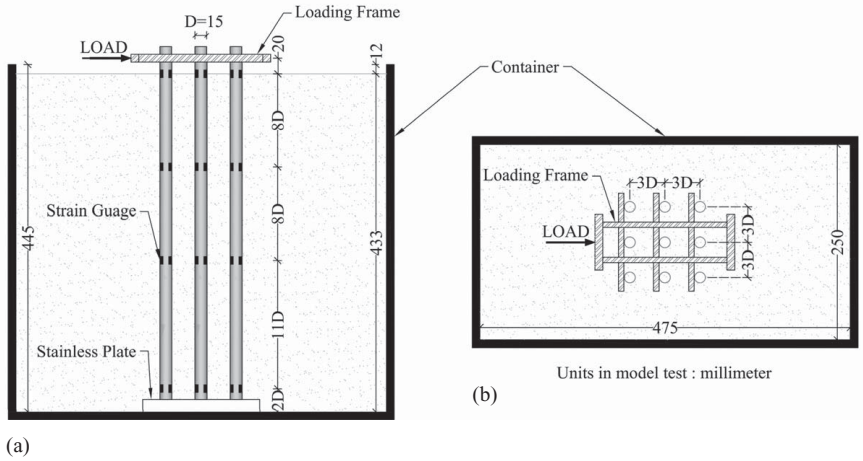

Fig. 11. Model setup in the centrifuge tests for static loading: (a) section view; and (b) plan view (Tobita et al. 2004).

Table 3. Piles characteristics in model and prototype scales in Tobita et al. (2004) study

Characteristic	Model scale	Prototype scale	Unit
Length	0.5	10	m
Outer diameter	15	300	mm
Wall thickness	1	20	mm
Elastic modulus	101	101	GPa
Moment of inertia	1.08×10^3	1.73×10^8	mm^4

lateral pile-head displacements as the single pile. An acceptable fit between the measured and computed bending moment profiles of the pile group is observed. The predicted value of the maximum bending moment matches well with that of the measurement, however the depth is over-predicted slightly. Presence of the clayey layers in shallow depths (lower than 10 pile diameter) might be the reason of inconsistency observed around the maximum bending moment location.

Case Study 3 (Centrifuge Test)

In an experimental study, Tobita et al. (2004) conducted centrifuge tests on both single piles and pile groups in a sand deposit to study the pile group behavior and to investigate *p-y* curves for seismic design based on the static tests data. A single pile and a 3×3 pile group at 3D pile spacing ($s = 0.9$ m) were tested under lateral loading. The single pile and the piles of the group had the same characteristics. Fig. 11 shows the centrifuge static test setup for the pile group model tests. The tubed piles in model and prototype scales were made up of brass. Table 3 lists the characteristics and dimensions of the piles for both model and prototype scales. Boundary conditions of the pile group were rotation-free at the head and rotation-fixed at the piles tips. The lateral load was applied to the single pile and pile group at the height of 0.02 and 0.4 m from the ground surface in the model and prototype scale, respectively. Hereafter, the prototype dimensions and characteristics are considered to validate the proposed method.

The piles were placed in 8.66 m silica sand deposit. Regarding the soil parameters, the maximum dry unit weight and the relative density of the silica sand were reported as $\gamma_d = 14$ kN/m^3 and $D_r = 65\%$ (medium dense), respectively. In their work, the soil friction angle ($\phi = 36°$) was approximated based on the relative density, without any measurement. Such a friction-angle value is controversial because the reported value does not match the unit weight as well as the mineralogy of the sandy deposit. Many studies in the literature have confirmed that the friction angle not only depends on density but also on mineralogy, as well as on consolidation stress (e.g., Sadrekarimi and Olson 2011; Schanz and Vermeer 1996). From the viewpoint of mineralogy, silica is the origin of quartz (Mitchell and Soga 2005), and the friction angle of the quartz sand is in the range of 27–32° (Bolton 1986; Budhu 2010). Furthermore, triaxial test results on quartz-origin sand with the consolidation stress of 100–200 kPa (similar to the stress levels that exists in the centrifuge tests performed by Tobita et al. (2004) indicate that the range of the friction angle is 26–30° (Sadrekarimi and Olson 2011). On the other hand, back analyses of the single pile behavior under lateral load give an estimation of $\phi = 29°$ for the silica sand. Consequently, it turns out that the value of $\phi = 36°$ is too high for the silica sand in the study of Tobita et al. (2004) and instead, $\phi = 29°$ is chosen in the present study. Based on the soil friction angle, $k = 3$ MN/m^3 is adopted according to the API (2002) recommended diagram. The elastic modulus of dry medium-dense sand is approximated in the range of 28–41 MPa, as stated by Callanan and Kulhawy (1985). Eventually, the value of $E^m = 30$ MPa is considered for the silica sand, assuming Poisson's ratio of $\nu^m = 0.3$.

Fig. 12 depicts the bending moment profiles of the single pile under different lateral displacements $\delta = 38.2$, 57.0, 74.2, 90.6, and 99.2 mm for both measured and calculated data. In the simulations, the soil was modeled by the Reese et al. (1974) *p-y* curves. Comparison of the results implies a very good agreement between the measured and predicted bending moment profiles. In all deformation levels, the location, as well as the magnitude of the maximum bending moment, are predicted accurately. A small underestimation can be recognized in the predictions, especially for small lateral displacements, though.

Similar to the foregoing case studies, required characteristics of the ESP is now computed following the steps 2–4 of the proposed procedure mentioned in the "Step-by-Step Procedure for Problem-Solving" section. The equivalent moment of inertia is assessed as $I_{eq} = 0.08706$ m^4 for the squared arrangement of the piles ($H = B = 2.1$ m), which gives $B_{eq} = H_{eq} = 1.011$ m and $E_{eq} = 567$ MPa. The L/B_{eq} ratio of the corresponding ESP is close to 10, which satisfies the geometry condition of the proposed method. The analysis of the pile group is achieved by using *p-y* models for the corresponding ESP. Fig. 13 illustrates the bending moment curves versus depth at five pile-head displacement levels, $\delta = 38.6$, 56.6, 74.2, 88.6, and 109.2 mm. The measured values from the tests are presented as well. Comparison between measured and computed results indicate that the overall shape of the bending moment

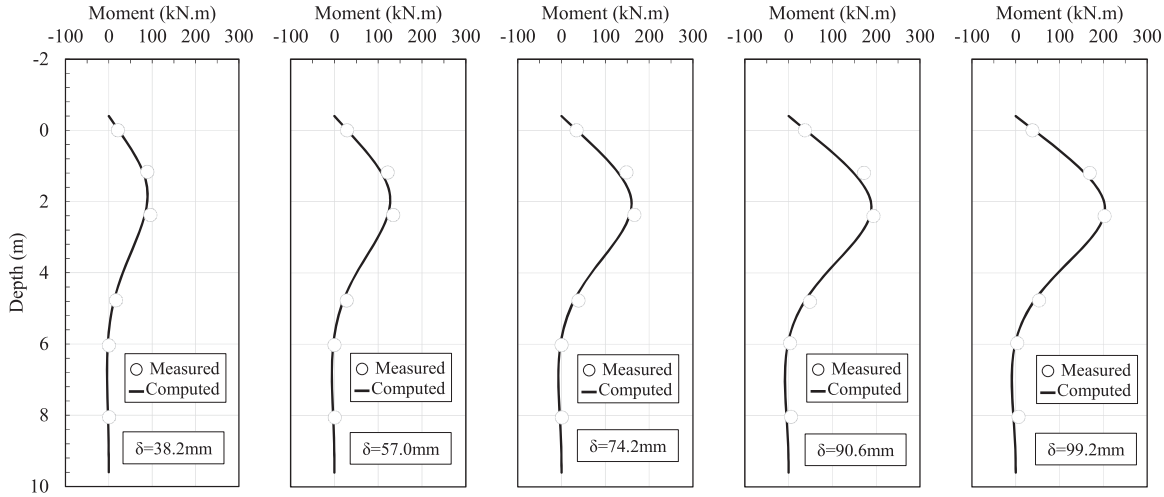

Fig. 12. Comparison of measured and computed bending moments versus depth at different pile-head deflection for the single pile test performed by Tobita et al. (2004).

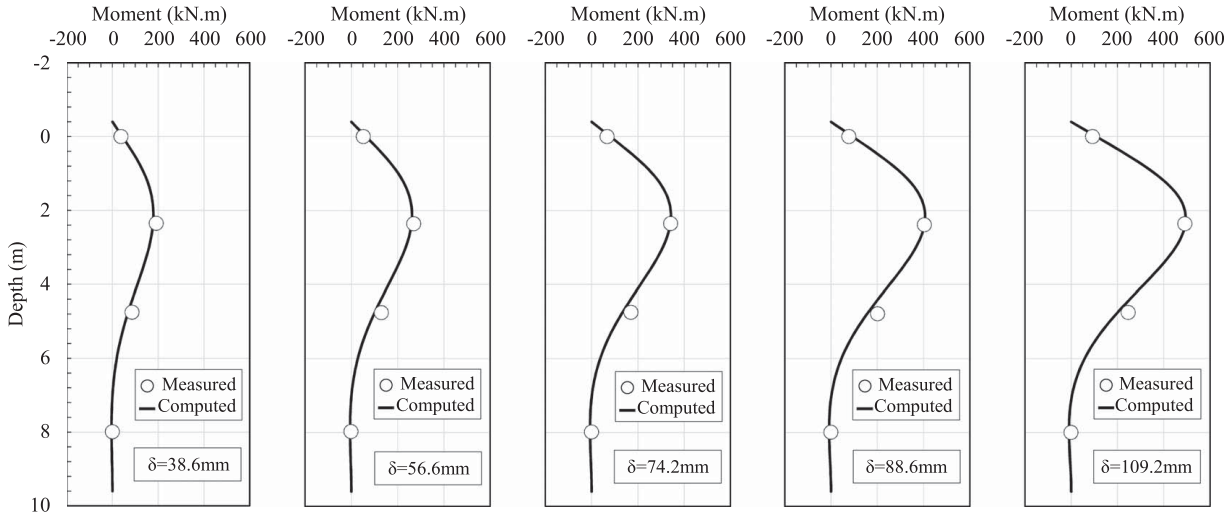

Fig. 13. Comparison of measured and computed bending moments versus depth at different pile-head deflection for the pile group test performed by Tobita et al. (2004) using the proposed method.

profile, as well as the location of the maximum bending moment, strongly agree. This case study also validates the capability of the proposed method in the analysis of laterally loaded pile groups.

Discussion

After validation of the proposed problem-solving algorithm, the importance of each parameter affecting the bending moment of the pile group is investigated. By referring to Eq. (30), note that the bending moment of the ESP is directly affected by the κ-multiplier. The effect of influencing parameters on the κ-multiplier is here discussed for a reasonable range.

During the description of the basic theory of elastic analysis for laterally loaded single piles, Poulos and Davis (1980) defined pile flexibility factor (K_R) as

$$K_R = \frac{E^I I^I}{2G^m(1+\nu^m)L^4} \tag{32}$$

K_R is a dimensionless measure of the flexibility of the pile relative to the surrounding soil and has no limiting value for an infinitely rigid pile, i.e., $K_R \to \infty$ and it reaches zero for an infinitely long pile. Generally, if $K_R > 0.02$, pile is considered as a rigid pile; otherwise, it would be flexible. By considering the K_R definition, the η parameter is rewritten as

$$\eta = \frac{s/D}{L/D}\sqrt{\frac{1}{2K_R(1+\nu^m)}} \tag{33}$$

Here, the formulation is intentionally presented in terms of normalized terms of s/D and L/D in order to investigate their effects on κ-multiplier directly.

According to typical values of K_R for various types of piles and soils reported by Poulos and Davis (1980), a reasonable range is $K_R = 10^{-6}$–1. A common range for pile spacing in the groups would be $s/D = 3$–6. A constant value of Poisson's ratio as $\nu^m = 0.3$ is also assumed.

By considering $L/D = 40$, similar to what existed in the case studies mentioned earlier ($L/D = 38.5$–41), the effect of pile spacing and the pile flexibility factor on the κ-multiplier can be investigated as shown in Fig. 14. In Fig. 14(a), the variation of the κ-multiplier with the pile spacing is illustrated for different pile-

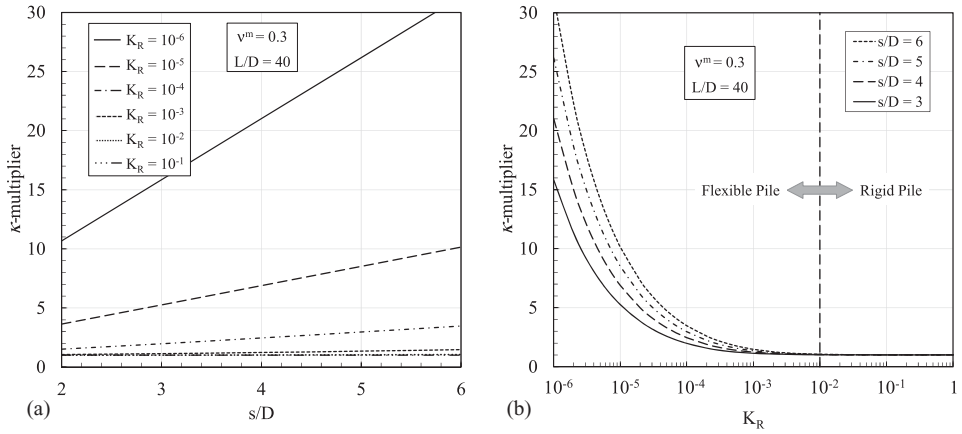

Fig. 14. Variation of κ-multiplier versus: (a) pile spacing (s/D); and (b) pile flexibility factor (K_R) for $\nu^m = 0.3$ and $L/D = 40$.

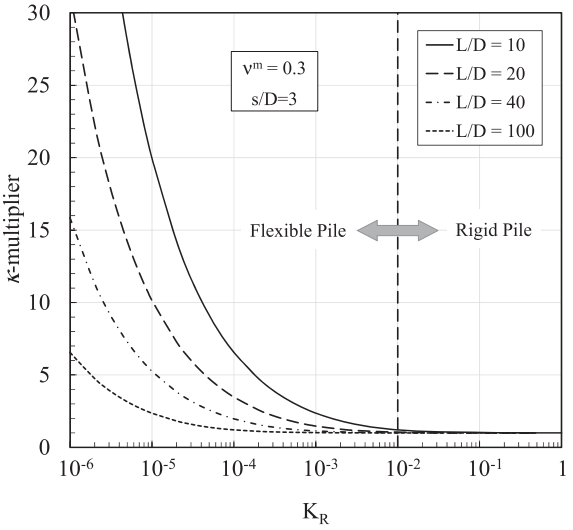

Fig. 15. κ-multiplier versus pile flexibility factor (K_R) for various L/D with $\nu^m = 0.3$ and $s/D = 3$.

flexibility factor magnitudes. It can be seen that the κ-multiplier grows gradually with s/D, whose rate is dependent on the pile flexibility factor. As the pile flexibility factor increases, the change of κ-multiplier decreases with s/D. Furthermore, for rigid piles ($K_R > 0.02$), the pile spacing has no effect on the κ-multiplier, and K_R tends to unity. However, for flexible piles with $K_R < 10^{-4}$, it is severely dependent on s/D. In other words, an increase of the pile spacing in a group reduces the group performance, and consequently the behavior of each pile becomes more similar to a single pile. Therefore, the κ-multiplier results in bigger values. From another viewpoint, the variation of κ-multiplier against the pile flexibility factor is plotted in Fig. 14(b). It is clear that κ-multiplier generally decreases exponentially with the pile flexibility factor reaching to one for rigid piles. It is noted that the pile spacing is more effective on the κ-multiplier value if $K_R < 0.02$ where κ-multiplier increases sharply as the pile becomes more flexible.

The influence of the pile flexibility factor on the value of the κ-multiplier for different pile length to diameter ratios (L/D), representing the slenderness of the piles of the group, is depicted in Fig. 15 by assuming a constant pile spacing equal to 3D ($s/D = 3$). As seen, the value of κ-multiplier is highly dependent to the pile flexibility factor if $K_R < 0.02$, regardless of the slenderness values of the pile. However, for rigid piles ($K_R > 0.02$), the κ-multiplier remains almost constant and has a small value around unity especially for very slender piles ($L/D \geq 100$). Nevertheless, the κ-multiplier grows quickly by decreasing L/D for flexible piles with $K_R < 10^{-3}$ and tends to infinity for less-slender flexible piles. Generally, κ-multiplier is highly dependent on the pile slenderness for L/D greater than 40.

Concluding Remarks

A new hybrid method for the analysis of laterally loaded pile groups founded in sandy soils was presented in this study. The proposed method is a combination of the two-phase approach and p-y curves to obtain the bending moment profile of a pile group under lateral load. The pile group and the soil among the piles are replaced by an ESP. The properties of the ESP are dependent on a parameter called as κ-multiplier, which is defined in terms of the bending stiffness of each pile, pile spacing, and the soil shear modulus. The ESP is analyzed by implementing an appropriate p-y model. Verification of the proposed method indicates an acceptable accuracy for predicted bending moment profiles. Major concluding remarks are summarized as:

- In contrast to existing p-y analyses of pile groups, any p-multipliers or other reduction factors are not required in the proposed analytical method. Rather, the response is predicted by implementing a unique p-y analysis for a single pile ESP whose properties represent those of the pile group.
- The proposed method requires a good estimation of the soil properties, by which the lateral response of a single pile can be accurately simulated.
- The proposed approach is appropriate only for the pile groups whose dimensions of the corresponding ESP satisfy the geometry criterion as $L/B_{eq} > 3$.
- The results of the reviewed case studies confirm that the proposed method can be safely applied to analyze the laterally loaded pile groups. Bending moment profile, as well as the location of the maximum bending moments, can be obtained properly by implementing such a simplified approach.
- The main parameter affecting the response of a laterally loaded pile group is the κ-multiplier, which is a function of the piles flexibility factor (K_R), slenderness (L/D), as well as pile spacing ratio (s/D).

Data Availability Statement

All data, models, and code that support the findings of this study are available from the corresponding author upon reasonable request (the data in the graphs and the code of calculation, etc.).

Notation

The following symbols are used in this paper:

A_1, A_2, A_3, and A_4 = constants of the solution in differential equation;
A_{eq} = cross-section area of the ESP;
A^*_{eq} = reduced cross-section area of the ESP;
A^I = cross-section area of an inclusion (and pile);
A^{*I} = reduced cross-section area of an inclusion (and pile);
B = pile group dimension along the y-axes;
B_{eq} = ESP dimension along the y-axes;
c = cohesion;
D = pile diameter;
D_r = soil relative density;
d = distance between the neutral axis of the pile group in plan view and each pile row axis;
E_{eq} = elastic modulus of ESP;
$\bar{E}_{eq}$ = weighted average value of E_{eq};
E^I = elastic modulus of an inclusion (and pile);
$(EI)_{eq}$ = ESP bending rigidity;
E^m = soil elastic modulus;
$\boldsymbol{e_x}$ = unit vectors along the x-axis;
$\boldsymbol{e_y}$ = unit vectors along the y-axis;
$\boldsymbol{e_z}$ = unit vectors along the z-axis;
$f^{ESP}(x)$ = displacement function of the ESP;
f_s = shape factor;
$f(x)$ = displacement function of a shear-loaded reinforced soil layer;
G_{eq} = shear modulus of the ESP;
$G_{eq}A^*_{eq}$ = ESP shear rigidity;
G^I = shear modulus of an inclusion (and pile);
G^m = shear modulus of the matrix (and soil);
H = pile group dimension along the z-axes;
H_{eq} = ESP dimension along the z-axes;
h = thickness of the soil layer;
I_{eq} = ESP moment of inertia about the z-axis;
I^I = moment of inertia of an inclusion (and pile);
$\boldsymbol{J}$ = interaction force vector;
K_R = pile flexibility factor;
k = lateral subgrade modulus;
L = pile length;
$M^r(x)$ = bending moment function in the reinforcement phase;
$M^{ESP}(x)$ = bending moment function of the ESP;
m^r = density of bending moment per unit area;
N = number of the soil layers;
n^r = density of axial force per unit area;
p = soil resistance;
q_c = cone resistance in the cone penetration test (CPT);
R = represent the shear behavior contribution in the ESP;
s = center to center pile spacing;
t = wall thickness of tubed pile;
v^r = density of shear force per unit area;
y = soil lateral displacement;
α^r = axial stiffness density per unit area of pile group;
β^r = shear stiffness density per unit area of pile group;
γ = soil unit weight;
γ' = effective soil unit weight;
γ_d = maximum dry unit weight;
γ^r = flexural stiffness density per unit area of pile group;
δ = applied horizontal displacement;
ε_{50} = strain corresponding to one-half of the maximum principal stress difference;
$\boldsymbol{\varepsilon^m}$ = strain tensor of matrix phase;
ε^r = axial strain of reinforcement phase;
η = relative stiffness density per unit area of the pile group;
η_1 = nondimensional parameter;
η_2 = nondimensional parameter;
θ^r = shear strain of reinforcement phase;
κ = κ-multiplier;
ν_{eq} = Poisson's ratio of the ESP;
ν^I = Poisson's ratio of an inclusion (and pile);
ν^m = Poisson's ratio of the matrix (and soil);
ξ = displacement field;
ξ^m = displacement fields of matrix phase;
ξ^r = displacement fields of reinforcement phase;
$\rho\boldsymbol{F}$ = vector of the external body force;
$\boldsymbol{\sigma^m}$ = classical Cauchy stress tensor;
ϕ = soil internal friction angle;
$\chi(x)$ = curvature function of a shear loaded reinforced soil layer;
$\chi^{ESP}(x)$ = curvature function of the ESP;
χ^r = curvature of the reinforcement phase;
ψ = similarity ratio;
$\omega^{ESP}(x)$ = rotation function of the ESP;
ω^r = rotation field of reinforcement phase; and
$\omega(x)$ = rotation function of a shear loaded reinforced soil layer.

References

Adhikary, D. P., and A. V. Dyskin. 1997. "A Cosserat continuum model for layered materials." *Comput. Geotech.* 20 (1): 15–45. https://doi.org/10.1016/S0266-352X(96)00011-0.

API (American Petroleum Institute). 2002. *Recommended practice for planning, designing and constructing fixed offshore platforms*. 2A(RP-2A). Washington, DC: API.

Ashford, S. A., and T. Juimarongrit. 2003. "Evaluation of pile diameter effect on initial modulus of subgrade reaction." *J. Geotech. Geoenviron. Eng.* 129 (3): 234–242. https://doi.org/10.1061/(ASCE)1090-0241(2003)129:3(234).

Bolton, M. D. 1986. "The strength and dilatancy of sands." *Géotechnique* 36 (1): 65–78. https://doi.org/10.1680/geot.1986.36.1.65.

Bourgeois, E., G. Hassen, and P. de Buhan. 2013. "Finite element simulations of the behavior of piled-raft foundations using a multiphase model." *Int. J. Numer. Anal. Methods Geomech.* 37 (9): 1122–1139. https://doi.org/10.1002/nag.2077.

Bourgeois, E., P. de Buhan, and G. Hassen. 2012. "Settlement analysis of piled-raft foundations by means of a multiphase model accounting for soil-pile interactions." *Comput. Geotech.* 46: 26–38. https://doi.org/10.1016/j.compgeo.2012.05.015.

Bowles, J. E. 1996. *Foundation analysis and design*. New York: McGraw-Hill Companies.

Brown, D. A., C. Morrison, and L. C. Reese. 1988. "Lateral load behavior of pile group in sand." *J. Geotech. Eng.* 114 (11): 1261–1276. https://doi.org/10.1061/(ASCE)0733-9410(1988)114:11(1261).

Budhu, M. 2010. *Soil mechanics and foundations*. Hoboken, NJ: Wiley.

Callanan, J. F., and F. H. Kulhawy. 1985. *Evaluation of procedures for predicting foundation uplift movements*. Palo Alto, CA: Electric Power Research Institute.

Caltrans. 1990. *Caltrans bridge design specifications/seismic design references*. Sacramento, CA: Caltrans.

Chen, J., Y. Huang, and M. Ortiz. 1998. "Fracture analysis of cellular materials: A strain gradient model." *J. Mech. Phys. Solids* 46 (5): 789–828. https://doi.org/10.1016/S0022-5096(98)00006-4.

Chen, Y. 1997. "Assessment on pile effective lengths and their effects on design—I. Assessment." *Comput. Struct.* 62 (2): 265–286. https://doi.org/10.1016/S0045-7949(96)00201-5.

Christensen, D. S. 2006. "Full scale static lateral load test of a 9 pile group in sand." Master thesis, Dept. Civil and Environmental Engineering, Brigham Young Univ.

Comodromos, E. M., and M. C. Papadopoulou. 2012. "Response evaluation of horizontally loaded pile groups in clayey soils." *Géotechnique* 62 (4): 329–339. https://doi.org/10.1680/geot.10.P.045.

de Buhan, P., E. Bourgeois, and G. Hassen. 2008. "Numerical simulation of bolt-supported tunnels by means of a multiphase model conceived as an improved homogenization procedure." *Int. J. Numer. Anal. Methods Geomech.* 32 (13): 1597–1615. https://doi.org/10.1002/nag.685.

de Buhan, P., and B. Sudret. 1999. "A two-phase elastoplastic model for unidirectionally-reinforced materials." *Eur. J. Mech. A. Solids* 18 (6): 995–1012. https://doi.org/10.1016/S0997-7538(99)00109-6.

de Buhan, P., and B. Sudret. 2000. "Micropolar multiphase model for materials reinforced by linear inclusions." *Eur. J. Mech. A. Solids* 19 (4): 669–687. https://doi.org/10.1016/S0997-7538(00)00181-9.

DNV (Det Norske Veritas). 1977. *Rules for the design, construction and inspection of offshore structures*. Oslo, Norway: DNV.

El Sharnouby, B., and M. Novak. 1985. "Static and low-frequency response of pile groups." *Can. Geotech. J.* 22 (1): 79–94. https://doi.org/10.1139/t85-008.

Fayyazi, M. S., M. Taiebat, and W. D. L. Finn. 2014. "Group reduction factors for analysis of laterally loaded pile groups." *Can. Geotech. J.* 51 (7): 758–769. https://doi.org/10.1139/cgj-2013-0202.

Hassen, G., and P. de Buhan. 2005. "A two-phase model and related numerical tool for the design of soil structures reinforced by stiff linear inclusions." *Eur. J. Mech. A. Solids* 24 (6): 987–1001. https://doi.org/10.1016/j.euromechsol.2005.06.009.

Hassen, G., D. Dias, and P. de Buhan. 2009. "Multiphase constitutive model for the design of piled-embankments: Comparison with three-dimensional numerical simulations." *Int. J. Geomech.* 9 (6): 258–266. https://doi.org/10.1061/(ASCE)1532-3641(2009)9:6(258).

Hetenyi, M. 1946. *Beams on elastic foundation*. Ann Arbor, MI: University of Michigan Press.

Isenhower, W., S. Wang, and J. Arrellaga. 2018. *User's manual for LPILE 2018, version 10*. Austin, TX: Ensoft.

Kitiyodom, P., and T. Matsumoto. 2002. "A simplified analysis method for piled raft and pile group foundations with batter piles." *Int. J. Numer. Anal. Methods Geomech.* 26 (13): 1349–1369. https://doi.org/10.1002/nag.248.

Kitiyodom, P., and T. Matsumoto. 2003. "A simplified analysis method for piled raft foundations in non-homogeneous soils." *Int. J. Numer. Anal. Methods Geomech.* 27 (2): 85–109. https://doi.org/10.1002/nag.264.

Leung, C. F., and Y. K. Chow. 1987. "Response of pile groups subjected to lateral loads." *Int. J. Numer. Anal. Methods Geomech.* 11 (3): 307–314. https://doi.org/10.1002/nag.1610110307.

Matlock, H. 1970. "Correlations for design of laterally loaded piles in soft clay." In *Proc., 2nd Offshore Technology Conf.*, 577–594. Richardson, Texas: Offshore Technology Conference.

McVay, M., R. Casper, and T.-I. Shang. 1995. "Lateral response of three-row groups in loose to dense sands at 3D and 5D pile spacing." *J. Geotech. Eng.* 121 (5): 436–441. https://doi.org/10.1061/(ASCE)0733-9410(1995)121:5(436).

McVay, M., L. Zhang, T. Molnit, and P. Lai. 1998. "Centrifuge testing of large laterally loaded pile groups in sands." *J. Geotech. Geoenviron. Eng.* 124 (10): 1016–1026. https://doi.org/10.1061/(ASCE)1090-0241(1998)124:10(1016).

Meyer, B. J., and L. C. Reese. 1979. *Analysis of single piles under lateral loading*. Austin, TX: Center for Highway Research, Univ. of Texas at Austin.

Mitchell, J. K., and K. Soga. 2005. *Fundamentals of soil behavior*. Hoboken, NJ: Wiley.

Nasrollahi, S. M., and E. Seyedi Hosseininia. 2019. "A simplified solution for piled-raft foundation analysis by using two-phase approach." *C. R. Méc.* 347 (10): 716–733. https://doi.org/10.1016/j.crme.2019.10.002.

Nguyen, V. T., G. Hassen, and P. de Buhan. 2016. "A multiphase approach for evaluating the horizontal and rocking impedances of pile group foundations." *Int. J. Numer. Anal. Methods Geomech.* 40 (10): 1454–1471. https://doi.org/10.1002/nag.2495.

Ooi, P. S. K., and J. M. Duncan. 1994. "Lateral load analysis of groups of piles and drilled shafts." *J. Geotech. Eng.* 120 (6): 1034–1050. https://doi.org/10.1061/(ASCE)0733-9410(1994)120:6(1034).

Pender, M. J. 1993. "A seismic pile foundation design analysis." *Bull. N. Z. Soc. Earthquake Eng.* 26 (1): 49–160. https://doi.org/10.5459/bnzsee.26.1.49-160.

Popov, E. P. 1998. *Engineering mechanics of solids*. London: Pearson.

Poulos, H. G. 2018. "Rational assessment of modulus of subgrade reaction." *Geotech. Eng. J. SEAGS & AGSSEA* 49 (1): 1–7.

Poulos, H. G., and E. H. Davis. 1980. *Pile foundation analysis and design*. Hoboken, NJ: Wiley.

Randolph, M. F. 1981. "The response of flexible piles to lateral loading." *Géotechnique* 31 (2): 247–259. https://doi.org/10.1680/geot.1981.31.2.247.

Reese, L. C., W. R. Cox, and F. D. Koop. 1974. "Analysis of laterally loaded piles in sand." In *Proc., 6th Annual Offshore Technology Conf.*, 473–485. Richardson, Texas: Offshore Technology Conference.

Reese, L. C., and W. F. Van Impe. 2010. *Single piles and pile groups under lateral loading*. Boca Raton, FL: CRC Press.

Rollins, K. M., J. D. Lane, and T. M. Gerber. 2005. "Measured and computed lateral response of a pile group in sand." *J. Geotech. Geoenviron. Eng.* 131 (1): 103–114. https://doi.org/10.1061/(ASCE)1090-0241(2005)131:1(103).

Ruesta, P. F., and F. C. Townsend. 1997. "Evaluation of laterally loaded pile group at Roosevelt Bridge." *J. Geotech. Geoenviron. Eng.* 123 (12): 1153–1161. https://doi.org/10.1061/(ASCE)1090-0241(1997)123:12(1153).

Sadrekarimi, A., and S. M. Olson. 2011. "Critical state friction angle of sands." *Géotechnique* 61 (9): 771–783. https://doi.org/10.1680/geot.9.P.090.

Schanz, T., and P. A. Vermeer. 1996. "Angles of friction and dilatancy of sand." *Géotechnique* 46 (1): 145–151. https://doi.org/10.1680/geot.1996.46.1.145.

Seyedi Hosseininia, E., and A. Ashjaee. 2018. "Numerical simulation of two-tier geosynthetic-reinforced-soil walls using two-phase approach." *Comput. Geotech.* 100: 15–29. https://doi.org/10.1016/j.compgeo.2018.04.003.

Seyedi Hosseininia, E., and O. Farzaneh. 2010a. "A simplified two-phase macroscopic model for reinforced soils." *Geotext. Geomembr.* 28 (1): 85–92. https://doi.org/10.1016/j.geotexmem.2009.09.009.

Seyedi Hosseininia, E., and O. Farzaneh. 2010b. "Development and validation of a two-phase model for reinforced soil by considering nonlinear behavior of matrix." *J. Eng. Mech.* 136 (6): 721–735. https://doi.org/10.1061/(ASCE)EM.1943-7889.0000111.

Seyedi Hosseininia, E., and O. Farzaneh. 2011. "A non-linear two-phase model for reinforced soils." In *Proc., Institution of Civil Engineers—Ground Improvement*, 203–211. London: ICE Publishing.

Shen, W. Y., and C. I. Teh. 2002. "Analysis of laterally loaded pile groups using a variational approach." *Géotechnique* 52 (3): 201–208. https://doi.org/10.1680/geot.2002.52.3.201.

Son, Q. T., G. Hassen, and P. de Buhan. 2010. "Seismic stability analysis of piled embankments: A multiphase approach." *Int. J. Numer. Anal. Methods Geomech.* 34 (1): 91–110. https://doi.org/10.1002/nag.816.

Sudret, B., and P. de Buhan. 2001. "Multiphase model for inclusion-reinforced geostructures: Application to rock-bolted tunnels and piled raft foundations." *Int. J. Numer. Anal. Methods Geomech.* 25 (2): 155–182. https://doi.org/10.1002/nag.123.

Teramoto, S., T. Niimura, T. Akutsu, and M. Kimura. 2018. "Evaluation of ultimate behavior of actual large-scale pile group foundation by in-situ lateral loading tests and numerical analysis." *Soils Found.* 58 (4): 819–837. https://doi.org/10.1016/j.sandf.2018.03.011.

Terzaghi, K. 1955. "Evalution of conefficients of subgrade reaction." *Géotechnique* 5 (4): 297–326. https://doi.org/10.1680/geot.1955.5.4.297.

Tobita, T., S. Iai, and K. Rollins. 2004. "Group pile behavior under lateral loading in centrifuge model tests." *Int. J. Phys. Modell. Geotech.* 4 (4): 01–11. https://doi.org/10.1680/ijpmg.2004.040401.

Vesic, A. B. 1961. "Beams on elastic subgrade and the Winkler's hypothesis." In *Proc., 5th Int. Conf. on Soil Mechanics and Foundation Engineering*, 845–850. London: International Society for Soil Mechanics and Geotechnical Engineering (ISSMG).

Wakai, A., S. Gose, and K. Ugai. 1999. "3-D elasto-plastic finite element analyses of pile foundations subjected to lateral loading." *Soils Found.* 39 (1): 97–111. https://doi.org/10.3208/sandf.39.97.

Walsh, J. M. 2005. "Full-scale lateral load tests of a 3 × 5 pile group in sand." Master thesis, Dept. Civil and Environmental Engineering, Brigham Young Univ.

Zhang, L., M. C. McVay, and P. Lai. 1999. "Numerical analysis of laterally loaded 3 × 3 to 7 × 3 pile groups in sands." *J. Geotech. Geoenviron. Eng.* 125 (11): 936–946. https://doi.org/10.1061/(ASCE)1090-0241(1999)125:11(936).

Zhao, T., and Y. Wang. 2018. "Interpretation of pile lateral response from deflection measurement data: A compressive sampling-based method." *Soils Found.* 58 (4): 957–971. https://doi.org/10.1016/j.sandf.2018.05.002.